Implementation of Dubin curves-based RRT* using an aerial image for the determination of obstacles and path planning to avoid them during displacement of the mobile robot.

Daniel Tenezaca B.[1], Christian Canchignia [1], Wilbert Aguilar[1], Dario Mendoza [1]

[1] Universidad de las Fuerzas Armadas - ESPE, Sangolquí, Ecuador
{hdtenezaca, cscanchignia, wgaguilar,djmendoza}@espe.edu.ec

Abstract. The application of mobile robots in autonomous navigation has contributed to the development of exploration tasks for the recognition of unknown environments. There are different methodologies for obstacles avoidance implemented in mobile robots, however, this research introduces a novel approach for a path planning of an Unmanned Ground Vehicle (UGV) using the camera of a drone to get an aerial view that allows to recognize ground features through image processing algorithms for detecting obstacles and target them in a determined environment. After aerial recognition a global planner with Rapidly-exploring Random Tree Star (RRT*) algorithm is executed, Dubins curves are the method used in this case for nonholonomic robots. The study also focuses on determining the compute time which is affected by a growing number of iterations in the RRT*, the value of step size between the tree's nodes and finally the impact of number of obstacles placed in the environment. This project is the initial part of a larger research about a Collaborative Aerial-Ground Robotic System.

Keywords: RRT*, Path planning, image processing.

1 Introduction

Unmanned Aerial Vehicles (UAVs) and mobile robots are used in different operations according to their performances. UAVs have many limitations, for example, the carrying capacity, flight time, etc. However, UAVs has a more ample range of vision of a workspace and higher velocities [1]. On the contrary, mobile robots present many advantages compared to UAVs. Mobile robots can carry heavier loads, have more power units, and higher capacity for processing [2] [3]. The purpose is to combine them to create a hybrid system taking into consideration the advantages of those two robotic systems. In this proposal, the UAV is able to analyze a broad portion of ground in specific workspace to provide safe displacement directions to the grounded vehicle [4] [5].

The research presents a study to establish a global planner that represents the data obtained from a top view generated by UAV [6]. First, the system develops an image through processing algorithms based on artificial vison in order to determinate the most relevant features inside the picture. In this case, the algorithm estimates the position of the obstacles as well as the mobile vehicle's destination.

LaValle [7] proposed RRT algorithm considered as an optimal technique to construct trajectories in nonconvex high-dimensional spaces and used to solve path planning problems. Commonly, an RRT is deficient to solve a problem related with the planning, therefore, it is necessary to implement a path planning algorithm based on that RRT* to expand the tree in free spaces [8]. The kinematic constraints of the ground vehicle based on Ackerman steering makes RRT* algorithm grows drawing curves easy to adapt the vehicle turning movements. This kind of curves is named Dubins path. Finally, it is important to consider adjusting many parameters to expand the tree, it will allow to know how the algorithm is affected when existing variations of the obstacles, number of iterations and the length of the connection between the tree's nodes.

In section 2, the article presents an image processing algorithm for constructing a global planner. In section 3, it details an analysis to stablish a RRT* algorithm using a geometrically method based on constructing tangent lines that connect two points with a shortest curve in a Euclidean plane. Finally in section 4 results will be presented according the data obtained in different scenarios and various obstacle configurations.

2 Image Processing

The main objective of image processing is to remark certain details on an image. For this reason, processing images from the UAV's camera is important to obtain a 2D binarized map where obstacles are recognized [9]. All stages are specified in the next flowchart:

Fig. 1. Flowchart image processing

2.1 Image acquisition

Parrot Bebop 2 was used as UAV. It has a 14-megapixel 'fisheye' with a 3-axis image stabilization system that maintains a fixed angle of the view. The drone's camera has to point to the ground (vertical position), for getting vertical camera's rotation we have used a software development kit provided by Robot Operating System (ROS). Experimental results show to an altitude of 4m above ground level our Region of Interest (ROI) covers an approximately metric area of 6m x 4m.

2.2 Changing Color spaces

Object discrimination using Red, Green and Blue color space (RGB) turns difficult because the object's color is correlated with the amount of light exposure at the moment. For that reason, Hue, Saturation and Value color space (HSV) is more relevant to discriminate colors regardless the amount of light at the scene. Change of color

spaces from RGB to HSV in this application allows better adapting of the obstacles' algorithm to light changes, in cases which shadows contribute to false positives [10].

2.3 Image smoothing

Noise reduction is a very important factor for good image processing. In this case, it is applied a Gaussian Blur filter [11]. This means that each pixel was affected for a kernel (neighbor pixels). A kernel of size 5 was used and a Gaussian kernel standard deviation in an X direction of 0, where the target is not to get a blurred image if else to eliminate the small percent of noise.

2.4 Binarization

In our application, it was important to separate foreground elements (obstacles) from the background of the image, binarization or thresholding methods are commonly used for that purpose [12]. The obstacles were considered the most outstanding element on the ground, therefore, establishing a binarized map where the obstacles have a pixel value of 0 and a pixel value of 1 is a free space. The Hue value which represents red color goes from 0^{o} – 30^{o} and 330^{o} – 0^{o} approximately. Another stage is using the binarization to detect the target blue [13].

2.5 Edge dilatation and erosion

The dilation convolution adds pixels to the boundaries of the obstacles' structure reducing noise, while erosion remove pixels on the outside boundaries of the obstacles' structure. The dilatation and erosion combined result in better filter. It fills holes (opening) and removes small objects (closing). The opening operation works with a structuring element a size kernel of 5. The operation affects the pixel and a 5x5 matrix size, meanwhile closing operation uses a size kernel of 21 [14].

3 RRT* Algorithm

Dubins curves-based RRT* is used as a global planner. It establishes the path by two type of configurations divided in Curve – straight – curve (CSC) and Curve- curve-curve (CCC), which are the pattern of expansion in the RRT* algorithm. Random sample paths are generated from combination of straight lines and curves.

3.1 Initial requirements

Data input to get the path with the RRT* algorithm serve as initial state and orientation, numbers of iterations, goal state, step size. To set Dubin curves parameters it is necessary to know the minimum turning radius of the robot. Finally, another important input data is having the binarized map (workspace).

3.2 RRT* Algorithm

Acording to Noreen et al [15] RRT* is based in a group of features which allow tree expansion very similar to RRT algorithm. The difference between the systems is that RRT* incorporates two special properties called near neighbor search and rewiring tree operations.

The algorithm is represented by a tree denoted as $T = (V, E)$, where V is a set of vertices and E is a set of edges. The initial configuration (q_{init}) includes a set of vertices that represents where the tree starts. In each iterations configured (Lines 3-11), the algorithm stablishes a random position (q_{rand}) in free region, $(q_{nearest})$ is searched in the tree according to predefined step size from (q_{rand}) and immediately the algorithm stablishes a new configuration (q_{new}) with $Steer$ function which guides the system from (q_{rand}) to $(q_{nearest})$. The function $Chooseparent$ allows to select the best parent node for the new configuration (q_{new}) before its insertion in tree considering the closest nodes that lie inside of a circular area, finding(q_{min}). Finally near neighbor operations allows to generate the optimal path repeating the previous process [16].

Table 1. Pseudocode RRT* algorithm

Algorithm RRT* **T = (V, E) ← RRT*** (q_{ini})	
1:	$T \leftarrow$ InitializeTree( );
2:	$T \leftarrow$ InsertNode$(\emptyset, q_{init}, \mathrm{T})$;
3:	***for*** i = 0 to i = N ***do***
4:	$q_{rand} \leftarrow$ Sample(i);
5:	$q_{nearest} \leftarrow$ Nearest(T, q_{rand});
6:	$(q_{new}, U_{new}) \leftarrow$ Steer$(q_{nearest}, q_{rand})$;
7:	***if*** Obstaclefree(q_{new}) ***then***
8:	$q_{near} \leftarrow$ Near$(T, q_{new}, \lvert V \rvert)$;
9:	$q_{min} \leftarrow$ Chooseparent $(q_{near}, q_{nearest}, q_{new})$;
10:	$T \leftarrow$ InsertNode(q_{min}, q_{new}, T);
11:	$T \leftarrow$ Rewire$(T, q_{near}, q_{min}, q_{new};)$
12:	***return*** T

3.3 Dubin Curves

The Dubin curves describes six types of trajectories: RSR, LSR, RSL, LSL, RLR, and LRL. Each configuration comes from an analogy that is denoted by R (right move), S (straight move) and L (left move) [17].

All these configurations use geometrically computing method based on constructing tangent lines between two circles. The first step has two circles C_1 and C_2, with their respective radius r_1 and r_2, where C_1 represents coordinates (x_1, y_1) and C_2 as (x_2, y_2) (see in Fig. 2).

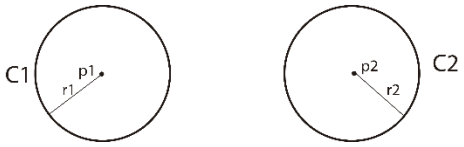

Fig. 2. Circles initial configuration

Inner tangents. Then a line is drawn between two center points C_1 and C_2 stablishing a vector $\overrightarrow{V_1}$, magnitude D and the midpoint p_3 (point between p_1 and p_2) is calculated , circle C_3 is constructed with a radius r_3 as we reflected in the Fig. 3

$$D = \sqrt{(x_2 - x_1)^2 + (y_2 - y_1)^2} \quad (1)$$

$$p_3 = (\frac{x_1+x_2}{2}, \frac{y_1+y_2}{2}) \quad (2)$$

$$r_3 = \frac{D}{2} \quad (3)$$

The next step is to draw another circle C_4 located in C_1's center, with radius $r_4 = r_1 + r_2$, we obtained p_t, which is the intersection between C_4 and C_3 like the one shown in Fig.3. A triangle is built joining the points p_1, p_3, p_t and we can define geometrically that segment $\overline{p_t p_1} = r_4$ and $\overline{p_1 p_3} = \overline{p_t p_3} = r_3$. The angle $\gamma = \angle p_t p_1 p_3$ is very important to define the coordinates of p_t. The next equation determinate the amount of rotation about the x-axis, θ for $\overrightarrow{V_2}$.

$$\theta = \gamma + atan2(\overrightarrow{V_1}) \quad (4)$$

Using θ, it is possible to obtain p_t according to the following equations:

$$x_t = x_1 + (r_1 + r_2) * \cos(\theta) \quad (5)$$

$$y_t = y_1 + (r_1 + r_2) * \sin(\theta) \quad (6)$$

Considering that the inner tangent starts on C_1, it is necessary to normalize a vector $\overrightarrow{V_2} = (p_t - p_1)$ and multiply it by r_1, the result will allow to find a vector $\overrightarrow{V_3}$ to p_{it1} from p_1. It resumes next by:

$$\overrightarrow{V_3} = \frac{\overrightarrow{V_2}}{\|V_2\|} * r_1 \quad (7)$$

$$p_{it1} = p_1 + \overrightarrow{V_3} \quad (8)$$

Finally, it is possible to draw a vector $\overrightarrow{V_4}$ from p_t to p_2, as shown in the figure. Using $\overrightarrow{V_4}$ magnitude and the direction it is possible to find the inner tangent point on C_2.

$$\overrightarrow{V_4} = (p_2 - p_t) \quad (9)$$

$$p_{it2} = p_{it1} + \overrightarrow{V_4} \quad (10)$$

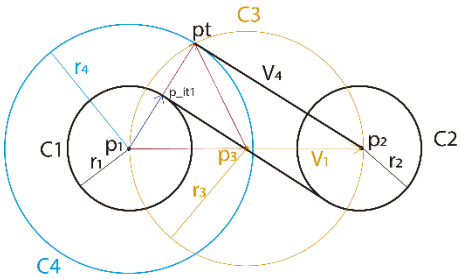

Fig. 3. Inner tangents

Outer tangents. The process is very similar to the one of inner tangents, having two circles C_1 and C_2, and considering $r_1 \geq r_2$, the procedure is the same as before, C_4 is centered at p_1, with a difference the radius $r_4 = r_1 - r_2$, after getting p_t and following all steps performed for the interior tangents, $\overrightarrow{V_2}$ is obtained and the first outer tangent point p_{ot1}. This condition produces that $r_4 < r_1$. To get the second outer tangent p_{ot2} an addition is performed by:

$$p_{ot2} = p_{ot1} + \overrightarrow{V_4} \qquad (11)$$

The main difference between calculating outer tangents compared to inner tangents is the construction of circle C_4; all steps keeps the same.

In the next figure (see Fig. 4), it can be seen the path establishes using data input.

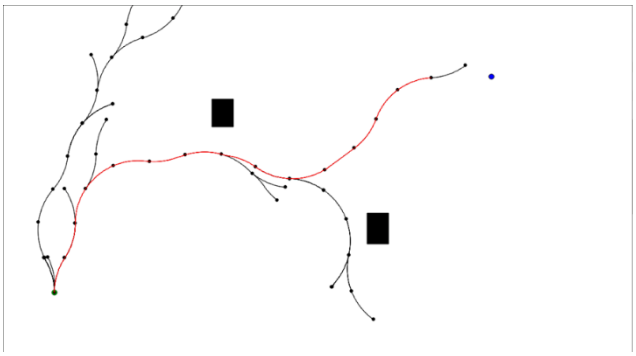

Fig. 4. RRT* algorithm's visualization

4 Results

The experimental results produced by RRT* path planning based on Dubins curves were performed using a CPU with an i7 third generation processor and 16 Gb RAM memory. For algorithm testing, a scene with a necessary amount of light was chosen to obtain the correct object segmentation. From this point the test started with no obstacles

in the scene. Then obstacles were gradually added to stablish four different configurations, in such way, algorithm functionality and efficiency was tested.

The algorithm was tested in 5 different cases (see Fig. 5), with no obstacles (first case), one obstacle (second case), two obstacles (third case), three obstacles (fourth case) and four obstacles (fifth case).

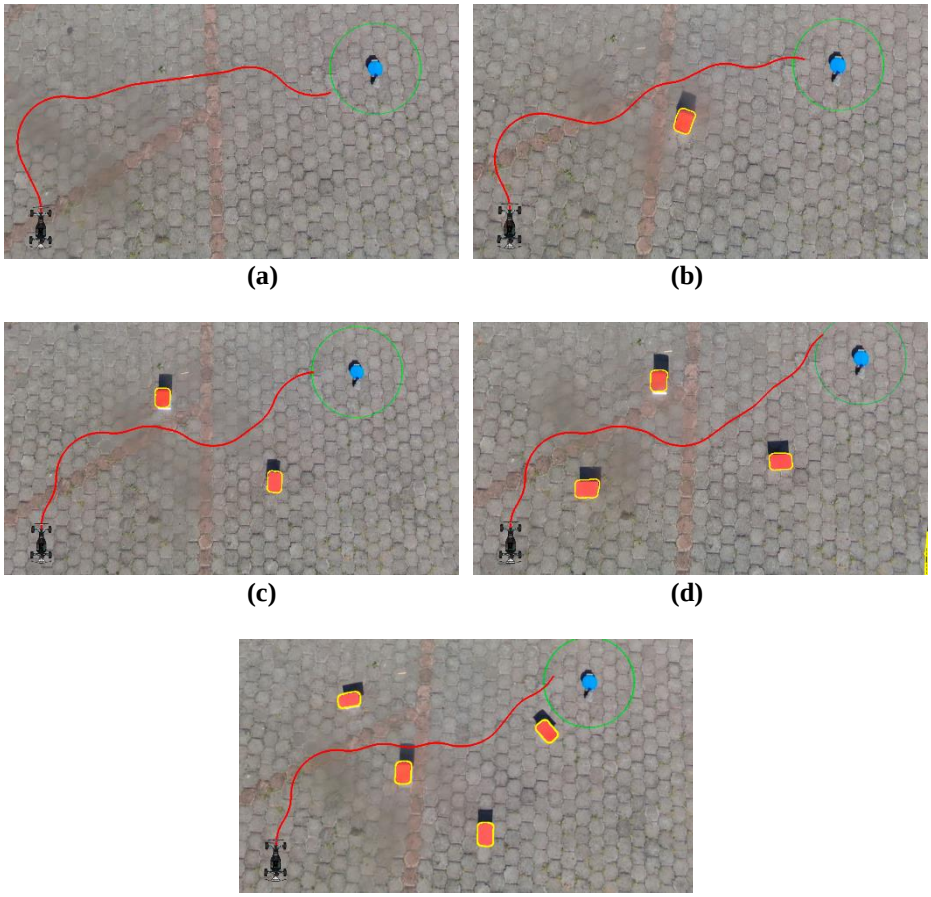

(a) **(b)** **(c)** **(d)** **(e)**

Fig. 5. Scene configurations

(a) No obstacles **(b)**One obstacle **(c)**Two obstacles **(d)**Three obstacles **(e)**Four obstacles

The algorithm satisfies its purpose because the path established (red line) started from car's position to the final configuration (blue circle) avoiding the obstacles. Another aspect to consider was that the goal position should have a tolerance radius of 60 pixels measured from the goal position's center point.

The first measurement of results (see Fig. 6) showed that the cases in which obstacles were added, it was necessary to increase the number of iterations to reach the configuration desired. Forty iterations were the minimum to reach the goal in the first case, compared with the fifth case where it was necessary at least 110 iterations to establish a path for UGV to represent.

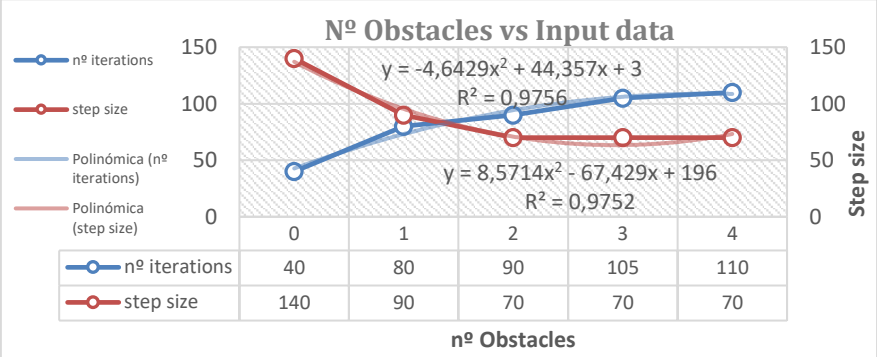

Fig. 6. Number of iterations and step size processed for each obstacle configuration

Based on the data processed, a second-grade polynomial equation was obtained to represent the number of iterations required for a scene where there are more than 4 obstacles in a scene.

$$y = -4{,}6x^2 + 44{,}3x + 3 \tag{12}$$

The ideal value for step size for each case is decreasing if we take into consideration the first test is with no obstacles and the fifth test has 4 obstacles in the scene. One-hundred-forty pixels the maximum step size for the optimal performance of the algorithm within the limits of workspace and for UGV to follow the path described. In the last three cases (case 3, case 4, and case 5), the necessary step size is 70 pixels, although the correlation of data is high by number of tests, the best possible solution in case the number of obstacles increase would be tested with the same value of step size.

Processing time required by the algorithm compared with the number of obstacles is presented in (Fig. 7). The blue line (time 1) describes the necessary time for expanding RRT* using an optimal data input for each case. The red one (time 2) describes the time required to reach de goal destination if the data is fixed with values of 30 pixels for step size and the maximum number of iterations is 1500.

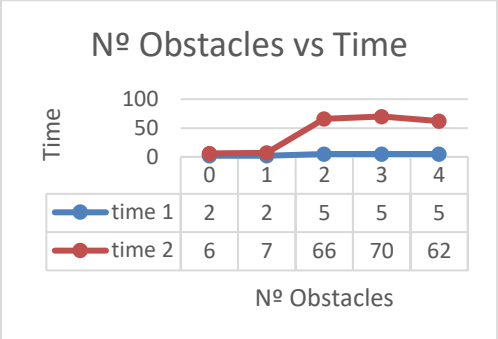

Fig. 7. Processing time required by algorithm

5 Conclusions

From the data aforementioned in this paper, we can conclude that exists a direct relationship between several iterations, step size, and quantity of obstacles. In case with few obstacles within the workspace, we can configure the step size in maximum value of 140 pixels allowing to reduce the number of times that mechanical direction of UGV has to rotate. The number of iterations are directly proportional to the number of obstacles because, more obstacles in the scene require to construct more iterations to reach the goal with an optimal path.

Establishing constant input data was not the most efficient way to execute the algorithm because if the step size configuration is too low, near 30 pixels, so the UGV can take an excessive time to follow the path and require too many changes in the direction of the robot.

This study has determined the importance of configuring initial parameters to construct the RRT* algorithm. Considering the path planning is based in a global planner, it is important to get the parameters in lesser time and optimal manner possible to obtain a better routing of data between UGV and UAV. Also, the study is the first stage of a global research for developing a collaborative robot system, we focused on getting a correct path for a mobile robot to navigate without colliding with objects around it. Finally, this work could be complemented with the development of pure pursuit control for UGV.

6 References

[1] D. Yulong, X. Bin, C. Jie, F. Hao, Z. Yangguang, G. Guanqiang y D. Lihua, «Path Planning of Messenger UAV in Air-ground Coordination,» *IFAC-PapersOnLine*, vol. 50, pp. 8045-8051, 2017.

[2] V. O.Sivaneri y J. N.Gross, «UGV-to-UAV cooperative ranging for robust navigation in GNSS-challenged environments,» *Aerospace Science and Technology*, vol. 71, pp. 245-255, 2017.

[3] R. Rahimi, F. Abdollahi y K. Naqshi, «Time-varying formation control of a collaborative heterogeneous multi agent system,» *Robotics and Autonomous Systems,* vol. 62, pp. 1799-1805, 2014.

[4] J. Melin, M. Lauri, A. Kolu, J. Koijonen y R. Ritala, «Cooperative Sensing and Path Planning in a Multi-vehicle Environment,» *IFAC-PapersOnLine,* pp. 198-203, 2015.

[5] L. Rosa, M. Cognetti, A. Nicastro, P. Alvarez y G. Oriolo, «Multi-task Cooperative Control in a Heterogeneous Ground-Air Robot Team,» *IFAC-PapersOnLine,* vol. 48, pp. 53-58, 2015.

[6] F. Ropero, P. Muñoz y M. D. R-Moreno, «TERRA: A path planning algorithm for cooperative UGV-UAV exploration,» *Engineering Applications of Artificial Intelligence,* 2019.

[7] S. LaValle, «The RRT Page,» 1999. [En línea]. Available: http://msl.cs.uiuc.edu/rrt/index.html.

[8] A. Abbadi y V. Prenosil, «Collided Path Replanning in Dynamic Environments Using RRT and Cell Decomposition Algorithms,» *Modelling and Simulation for Autonomous Systems: Second International Workshop,* pp. 131-143, 2015.

[9] T. Sieberth, R. Wackrow y J. H. Chandler, «Automatic detection of blurred images in UAV image sets,» *ISPRS Journal of Photogrammetry and Remote Sensing,* vol. 122, pp. 1-16, 2016.

[10] V. Chernov, J. Alander y V. Bochko, «Integer-based accurate conversion between RGB and HSV color spaces,» *Computer & Electrical Engineering* , vol. 46, pp. 328-337, 2015.

[11] J. Huang, H. Feng, Z. Xu, Q. Li y Y. Chen, «A robust deblurring algorithm for noisy images with just noticeable blur,» *Optik,* vol. 168, pp. 577-589, 2018.

[12] S. Chen y D. Li, «Image binarization focusing on objects,» *Neurocomputing,* vol. 69, pp. 2411-2415, 2006.

[13] E. Dougherty, Mathematical Morphology in image processing, Nueva York: Marcel Dekker, 1993.

[14] OpenCV, «OpenCV 2.4.13.7 documentation,» [En línea]. Available: https://docs.opencv.org/2.4/modules/imgproc/doc/filtering.html.

[15] I. Noreen, A. Khan y Z. Habib, «Comparison of RRT, RTT* and RRT*-Smart Path Planning Algorithms,» *IJCSNS International Journal of Computer Science and Network Security,* 2016.

[16] S. Karaman y E. Frazzoli, «Sampling-based algorithms for optimal,» *The International Journal of Robotic Research,* 2011.

[17] W. Yao, N. Qi, J. Zhao y N. Wan, «Bounded curvature path planning with expected length for Dubins vehicle entering target manifold,» *Robotics and Autonomous Systems,* vol. 97, pp. 217-229, 2017.